Dynamic identification and model updating of an eight-storey CLT building

Angelo Aloisio[a,*], Dag Pasca[b,*], Roberto Tomasi[b], Massimo Fragiacomo[a]

[a] *Department of Civil, Construction-Architectural and Environmental Engineering, Università degli Studi dell'Aquila, Via G. Gronchi, 18, L'Aquila, 67100, Abruzzo, Italy*
[b] *Faculty of Science and Technology, Norwegian University of Life Sciences, Oslo, Norway*

Abstract

So far, few in situ tests have been carried out to estimate the modal parameters of multi-storey Cross-Laminated-Timber (CLT) buildings: the understanding of their dynamic behaviour under operational conditions is still an open issue. In this paper, the results of the dynamic identification of an eight-storey CLT building are reported and interpreted in the light of a simplified shear-type analytical model. The structural model is calibrated on the experimental modal parameters, which are assessed using the Stochastic Subspace Identification (SSI). The SSI provides mode shapes, natural frequencies and damping factors of the structures in its first linear response range; The minimum of a modal-based objective function gives an estimation of the unknown parameters of the structural model. Given the results of the dynamic identification, the storey-masses are the chosen optimization parameters: the values of the experimental eigenfrequencies likely reveal a continuum-like behaviour of the building without connections. The identified storey masses are indeed realistic and confirm the negligible role of the connections in the low-amplitude dynamic response. The nonlinear effects of connections over the building response to higher displacements are discussed, providing simplified and practice-oriented correlations for the first natural frequency estimation.

Keywords: Dynamic Identification; Model Updating; CLT buildings; Nonlinear response

1. Introduction

Developments at the beginning of the 20th century made it possible to use reinforced concrete economically, and traditional timber constructions [1, 2] (log or stave

*Corresponding author.
Email addresses: angelo.aloisio1@graduate.univaq.it (Angelo Aloisio), dag.pasquale.pasca@nmbu.no (Dag Pasca), roberto.tomasi@nmbu.no (Roberto Tomasi), massimo.fragiacomo@univaq.it (Massimo Fragiacomo)

February 28, 2020

construction or lattice work) were successively superseded by the mineral-based solid construction materials concrete and brick, at least in Europe [3]. However, over the last 10 years or so, timber has recaptured market shares from the mineral-based solid construction materials, in particular in the fields of residential buildings, office buildings and schools but also other fields of construction. One reason for this development is the increasing interest in high-rise structures: the so-called "tall buildings". They require a higher level of seismic performance, leading to the use of massive and more effective systems, such as Cross-Laminated Timber (CLT) [4]. However, for the construction of larger and taller CLT buildings, it is necessary to understand their dynamic behaviour: movements, which may be acceptable for small heights and spans, are magnified in large structures, and may cause discomfort to building occupants, damage to non-structural elements, or increased loads on elements [5].

Aside from a few studies [5–8], the majority of research into the dynamic response of multi-storey CLT buildings has been under seismic loading: experiments and numerical modelling of CLT have been deeply investigated [4, 9–12], but the response to small-amplitude vibration is still an open issue. Reynolds et al. [5] obtained the modal parameters of a five-storey CLT building with an internal RC core. To fill a gap in knowledge, the authors present the dynamic identification of an eight-storey CLT building with a CLT core.

The estimate of the modal parameters of multi-storey CLT buildings' response under operational conditions from *in situ* tests is useful to understand the gap between the possibly linear dynamic response to service loading and nonlinear behaviour under seismic excitation. This gap is much wider for CLT buildings rather than concrete or steel buildings since the bearing resistance to lateral loads is concentrated in the connections (hold-downs and angle brackets e.g.), which are used for the building assemblage. The main objectives of this paper are: (i) the estimation of the modal parameters of an eight-storey CLT building from Output-Only dynamic identification; (ii) the updating of an elementary analytical model of the building to the experimental modal parameters; (iii) the assessment of the role of the connection nonlinearities on the building's dynamic response in operational conditions; (iv) the derivation of simplified and practice-oriented correlations useful for the assessment of natural frequencies and damping factors of CLT buildings at a low-level response.

2. Test building description

The eight-story case study building (Fig.1(a)) is in the NMBU campus (Norwegian University of Life Science), located in Ås, Norway. It has eight storeys with a total height of 26.9 m and is rectangular in plan (23.21 m × 15.11 m), with a CLT core at the centre. A plan of the building, indicating its structure, is shown in Fig.1(c), and an elevation showing the floor levels is given in Fig.1(b).

The tested building is made of large monolithic walls with high length-to-height ratios, assembled by tie-downs and shear connectors.

Table 1: Basic characteristics of the tested building [13].

Parameter	**Value**	**Unit**
Lenght	23.21	m
Width	15.11	m
Height	26.9	m
No. of floors	8	
Rooms	127	
Net area /floor	350.55	m^2
Net area /building	2804.4	m^2
CLT wall panels	3 layers-90 mm 5 layers-100,120,130, 140,160,180 mm	
CLT floor panels	5 layers-180,220 mm	
CLT roof panels	5 layers-200 mm	
Wood amount-total	907.62	m^3
Hold-downs steel plates	6225.73	Kg
Shear steel plates	1919	Kg
Self-tapping screws	6124	
Steel brackets	≈390	

The total lengths of the designated shear walls in the longitudinal and transverse directions are approximately 21,5m and 25m, respectively, excluding the partition walls, see Fig.1(d) [13]. Shear forces are being distributed using shear plates and brackets while long steel plates, ranging from the foundation to the roof, are placed at each end of the shear walls [13]. The main characteristics of the building are reported in Tab.1. The building currently houses student apartments in eight floors of similar layout.

3. Dynamic identification

The Stochastic Subspace identification method is used for the estimate of modal parameters from Output Only measurements [14–16].

(a)

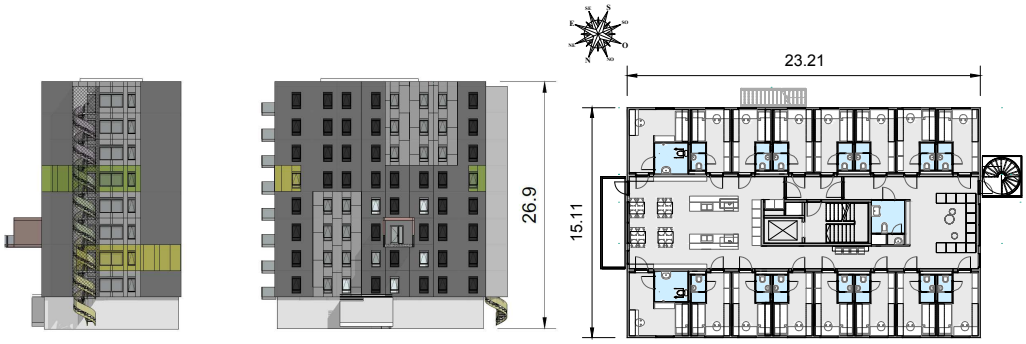

(b) (c)

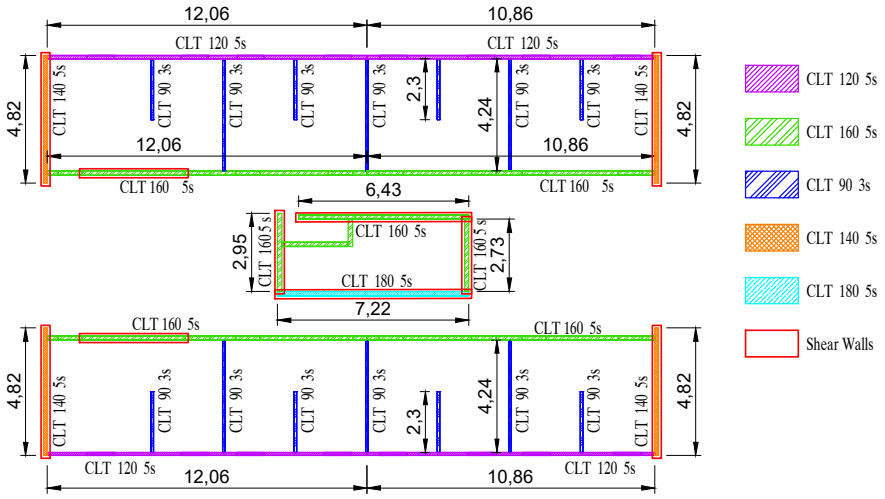

(d)

Figure 1: (a) North view of the building; (b) Prospects and plan (c)-(d) of the building.

3.1. Theoretical background

The SSI technique is a classical covariance-driven stochastic realization algorithm, namely the Principal Component algorithm [17, 18], also known as the covariance-driven SSI algorithm (SSIcov), that was generalized to a reference-based version (SSI-cov/ref) by Peeters and De Roeck [19–22].

State-space representation of output-only vibration-based structural monitoring corresponds to the following discrete time model

$$\begin{aligned} x_{k+1} &= Ax_k + v_k \\ y_k &= Cx_k + w_k \end{aligned} \tag{1}$$

with the states $x_k \in \mathbb{R}^n$, the outputs $y_k \in \mathbb{R}^r$, the state transition matrix $A \in \mathbb{R}^{n\times n}$ and the observation matrix $C \in \mathbb{R}^{r\times n}$, where r is the number of sensors and n is the system order. The excitation v_k is an unmeasured Gaussian white noise sequence with zero mean and constant covariance matrix $Q = \boldsymbol{E}(v_k v_k^T) \stackrel{\text{def}}{=} Q\delta(k-k')$, where $\boldsymbol{E}(\cdot)$ denotes the expectation operator and w_k is the measurement noise.

The algorithm starts with the construction of a block Toeplitz matrix of output covariance matrices, constructed with the l measured outputs and the r reference outputs:

$$L_{l,i}^{\text{ref}} \stackrel{\text{def}}{=} \begin{bmatrix} \Lambda_i^{\text{ref}} & \Lambda_{i-1}^{\text{ref}} & \dots & \Lambda_1^{\text{ref}} \\ \Lambda_{i+1}^{\text{ref}} & \Lambda_i^{\text{ref}} & \dots & \Lambda_2^{\text{ref}} \\ \vdots & \vdots & \ddots & \vdots \\ \Lambda_{2i-1}^{\text{ref}} & \Lambda_{2i-2}^{\text{ref}} & \dots & \Lambda_i^{\text{ref}} \end{bmatrix}, L_{l,i}^{\text{ref}} \in \mathbb{R}^{il\times ir} \tag{2}$$

where $\Lambda_j^{\text{ref}} = \boldsymbol{E}(y_k y_k^{\text{ref}\,T})$ is the covariances between all outputs y_k and some reference outputs. This matrix decomposes as

$$L_{l,i}^{\text{ref}} \stackrel{\text{def}}{=} \begin{bmatrix} C \\ CA \\ \vdots \\ CA^{i-1} \end{bmatrix} \begin{bmatrix} A^{i-1}G^{\text{ref}} & A^{i-2}G^{\text{ref}} & \dots & G^{\text{ref}} \end{bmatrix} \stackrel{\text{def}}{=} O_i C_i^{\text{ref}} \tag{3}$$

where $O_i \in \mathbb{R}^{il\times n}$ is called the extended observability matrix, $C_i^{\text{ref}} \in \mathbb{R}^{n\times ir}$ the reference-based stochastic controllability matrix, $G^{\text{ref}} = A\Sigma C^{\text{ref}T}$, $\Sigma = \boldsymbol{E}[x_k x_k^T]$ and n is the system order. The system matrices $A \in \mathbb{R}^{n\times n}$ and $C \in \mathbb{R}^{n\times l}$ can be derived as follows:

$$\begin{aligned} A &= (S_2 O_i)^{\dagger}(S_1 O_i) \\ C &= S_3 O_i \end{aligned} \tag{4}$$

where S_1, S_2 and S_3 are selection matrices:

$$S_1 = [0_{(i-1)l\times l} I_{(i-1)l}]; S_2 = [I_{(i-1)l} 0_{(i-1)l\times l}]; S_3 = [I_l 0_{l\times(i-1)l}] \tag{5}$$

The system's modal parameters (eigenfrequencies, damping ratios and mode shapes) can be calculated from the identified system description A, C.

$$A = \Psi\Lambda\Psi^{-1},\ A\psi_i = \lambda\psi_i \tag{6}$$

The undamped eigenfrequencies f_i and damping ratios ξ_i in % can be calculated from the dicrete-time poles λ_{ci}:

$$\lambda_{ci} = \frac{ln(\lambda_i)}{\Delta T},\ f_i = \frac{|\lambda_{ci}|}{2\pi},\ \xi_i = -100\frac{\lambda_{ci}^R}{|\lambda_{ci}} \tag{7}$$

where $|\cdot|$ denotes the complex modulus and $\lambda_{ci} = \lambda_{ci}^R + i\lambda_{ci}^I$. The observed part of the eigenvectors ψ_i leads to the experimental mode shapes ϕ_i:

$$\Phi = C\Psi,\ \phi_i = C\psi_i \tag{8}$$

3.2. Experimental setup

On October 25, 2019, the structure was subject to ambient vibration measurements. A set of 10 piezoelectric accelerometers was used Fig.2(a): 6 accelerometers, which provided a reference location [23], were placed on the rooftop, see Fig.2(c), while the other 4 were placed in the inferior floors in the 1 and 2 measurement points, Fig.2(c). Specifically, four tests were then carried out and five floors were tested, from the roof to the 5th elevation. The accelerometers were arranged to measure acceleration in two orthogonal directions, Fig.2(b). In order to confirm the

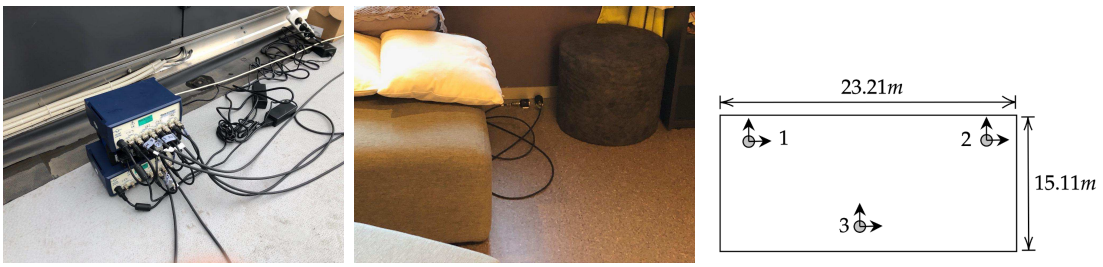

(a) (b) (c)

Figure 2: (a) Signal conditioner and DAQ system of the 10 IEPE piezoelectric accelerometers; (b) View of a couple of accelerometers measuring in two orthogonal directions; (c) Schematic view of the experimental setup of the rooftop.

assumption of horizontal rigid diaphragms, a redundant number of measurements

points on each floor was used.
The accelerometers PCB model 393B12 have a sensitivity of approximately 10000 mV/g, a frequency range from 0.15 Hz to 1000 Hz and a measurement range up to 10 m/s^2. The data were sampled at a rate of 100 Hz. The cut-off frequency of the anti-aliasing filter was set to 10 Hz. The number of samples was set to N=360000, which resulted in a measurement time of 1 hour. Data from multi-setup measurements (4 setups) were then merged following the approach recalled in. [24].

3.3. Results

Three stable frequencies clearly arise from the stabilization diagram [19] in the frequency range 0-10 Hz, Fig.3(d). The first three modes are evidenced by the peaks of the FFT of the signals in two orthogonal sensors, Fig.3(b)-(c). The variance of the acquired signal is approximately equal to $1.4 \times 10^{-5}\ m/s^2$ Fig.3(a): the low excitation is due to the wind, which blew at an approximate speed of $6\,Km/h$ with a NNE direction. The first two modes are translational: the very first at $1.913\,Hz$,

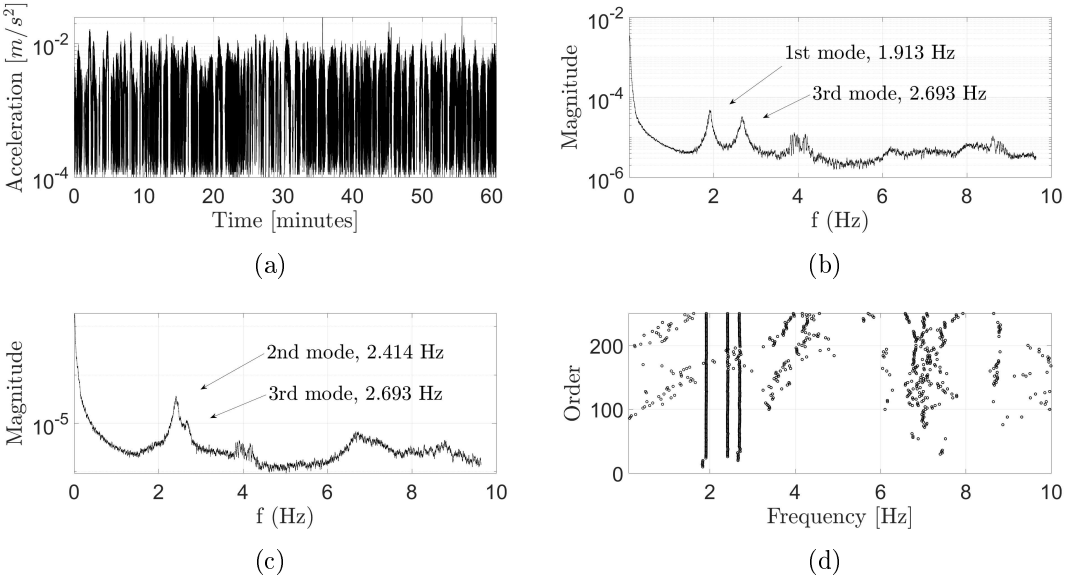

Figure 3: (a) Acceleration time-history of a reference accelerometer placed on the rooftop; (b)-(c) FFT of the signals in two orthogonal directions; (d) Stabilization diagram of the merged signals. The stabilization criteria are: $\delta f_i \leq 1\%$, $\delta \xi_i \leq 1\%$, MAC<1% [25].

Fig.4(a), is a translation parallel to the direction of minor inertia of the building; The second mode at $2.414\,Hz$ is a translation in the orthogonal direction, Fig.4(b). The third mode at $2.688\,Hz$ can be regarded as the first torsional mode, Fig.4(c). The damping factors range between 1.2-1.9%: the first modes are less damped than the other two, whose damping is almost close to 2%. Besides, a 2% damping can be considered in accordance with the standards predictions [26]. Two relevant aspects should be remarked:

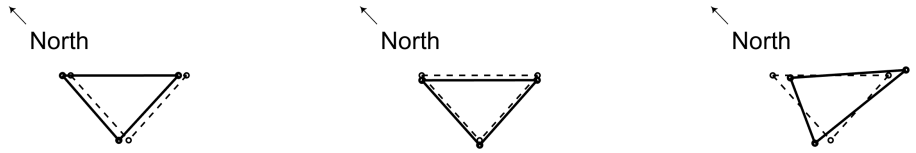

(a) 1st mode1.913 Hz; ξ = 1.216% (b) 2nd mode 2.414 Hz; ξ = 1.916% (c) 3rd mode 2.688 Hz; ξ = 1.921%

Figure 4: Natural frequencies, damping factors and mode shapes of the three stable modes in the frequency range $0 - 10\,Hz$ corresponding to the roof setup.

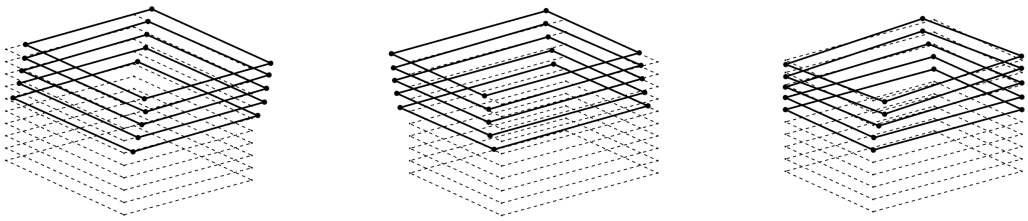

(a) 1st mode (b) 2nd mode (c) 3rd mode

Figure 5: Natural frequencies, damping factors and mode shapes of the three stable modes in the frequency range $0 - 10\,Hz$ corresponding to merged data sets.

- The CLT floors behave like rigid diaphragms;
- As later evidenced by the model updating, the natural frequencies are very high, as if the global stiffness of the building was due to the in-plane deformability of the sole CLT panels, without the contribution of the connections. At a very low vibration level, the building may behave like a rigid "box-like" structure: the amplitude of the excitation might not be enough to activate the uplift of the tie-downs nor to overcome the initial slip of the shear connectors.

The behaviour of timber structural systems and their connections is substantially nonlinear at low loads as well as high [6], as evidenced by experimental cyclic tests on CLT panels; However, very low excitation levels, like the ones of the current tests, are not considered in experimental cyclic tests [9]: below a certain displacement threshold, the CLT building may behave almost linearly, like a continuum.
However, the assessment of the nonlinear or possibly non-stationary behaviour of CLT buildings in operational conditions cannot be derived from dynamic identification tests. A continuous monitoring would be needed to appreciate the actual behaviour at low vibration levels under different values of the excitation (wind, e.g.). So far, there is a lack of knowledge on the Structural Health Monitoring

(SHM) of high-rise CLT buildings and more researches on this topic are needed.

Given the diaphragm-like behaviour of the CLT floors, a linear analytical model is used to interpret the experimental results and better understand the aspects remarked in this section. Detailed modelling of the CLT building is an important issue to be investigated in future researches, but it is not the purpose of this paper.

4. Model updating

An elementary shear-type 3-D building model [27] is presented and then calibrated to the experimental results by minimizing a proper objective function. The values of the experimental eigenfrequencies and the considerable in-plane stiffness of the CLT floors drove the choice towards the stiffest structural model: the shear-type one. However, the availability of accelerometers in the out-of-plane floor direction would have let to rigorously assess the approximation in using the shear-type rather than the cantilevered model. In practical situations, the selection of the structural model can profoundly affect the prediction of dynamic properties [28, 29], yielding a wide range of natural frequencies. For this reason, the designer should carefully ponder the choice of the model based on the expected structural response in relation with the considered limit state and the type of excitation (wind, seismic load, e.g.).

4.1. Model description

The equations of motion of a generic 2D storey are derived, then the resulting mass and stiffness matrices are assembled into the mass and stiffness matrices of the whole structure.
It is assumed that a generic storey is supported by N structural elements. The

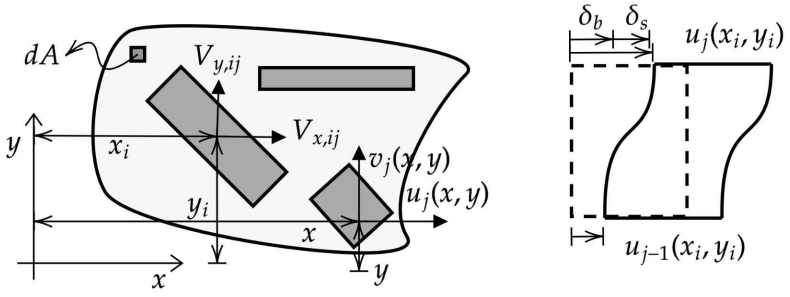

Figure 6: Plan view of a general configuration of the bearing walls of the j-th storey.

equilibrium (Eq.9), compatibility (Eq.10) and constitutive (Eq.11) equations of a

j-th storey can be written as:

$$\begin{gathered}\sum_{i=1}^{N} V_{x,ij} + \int_{A_j} \rho_j(x,y)\, \ddot{u}_j(x,y)\, dA = 0 \\ \sum_{i=1}^{N} V_{y,ij} + \int_{A_j} \rho_j(x,y)\, \ddot{v}_j(x,y)\, dA = 0 \\ -\sum_{i=1}^{N} V_{x,ij} y_i + \sum_{i=1}^{N} V_{y,ij} x_i + \int_{A_j} \rho_j(x,y)\, y\, \ddot{u}_j(x,y)\, dA - \int_{A_j} \rho_j(x,y)\, x\, \ddot{v}_j(x,y)\, dA = 0\end{gathered} \tag{9}$$

$$\begin{aligned} u_j(x,y) &= u_{0j} - \theta_j y \\ v_j(x,y) &= v_{0j} + \theta_j x \end{aligned} \tag{10}$$

$$\begin{aligned} V_{x,ij} &= k_{x,ij}\left(u_j(x_i,y_i) - u_{j-1}(x_i,y_i)\right) \\ V_{y,ij} &= k_{y,ij}\left(v_j(x_i,y_i) - v_{j-1}(x_i,y_i)\right) \end{aligned} \tag{11}$$

where $V_{x,ij}$ and $V_{y,ij}$ are the shear components in the x and y direction of the i-th wall of the j-th storey, $\rho_j(x,y)$ is the mass per unit square, $u_j(x,y)$ and $v_j(x,y)$ are the displacement components in the x and y direction, dA is the infinitesimal element area and A_j the total area of the storey, Fig.(6).
The compatibility equations are written assuming the diaphragm-like behaviour of each floor, while the constitutive equations are based on the estimation of two shear stiffness values in the x and y directions, $k_{x,ij}$ and $k_{y,ij}$ respectively, concentrated in the centre of mass of each wall. The undamped equilibrium equations of the j-th storey in terms of displacements can be then written as follows:

$$M_j \ddot{v}_j + K_j v_j = 0 \tag{12}$$

$$v_j = \begin{bmatrix} u_{0,j} \\ v_{0,j} \\ \theta_j \end{bmatrix}^{\mathrm{T}} \quad M_j = \begin{bmatrix} M_{xx,j} & 0 & -M_{xy,j} \\ 0 & M_{yy,j} & M_{yx,j} \\ -M_{xy,j} & M_{yx,j} & I_{M,j} \end{bmatrix} \quad K_j = \begin{bmatrix} K_{xx,j} & 0 & -K_{xy,j} \\ 0 & K_{yy,j} & K_{yx,j} \\ -K_{xy,j} & K_{yx,j} & I_{K,j} \end{bmatrix} \tag{13}$$

where $M_{xx,j} = M_{yy,j} = \int_{A_j} \rho_j(x,y)dA$, $M_{xy,j} = \int_{A_j} y\rho_j(x,y)dA$, $M_{yx,j} = \int_{A_j} x\rho_j(x,y)dA$, $I_{M,j} = \int_{A_j} (x^2+y^2)\,\rho_j(x,y)dA$, $K_{xx,j} = \sum_{i=1}^{N} x_i^2 k_{x,ij}$, $K_{yy,j} = \sum_{i=1}^{N} y_i^2 k_{y,ij}$, $I_{K,j} = \sum_{i=1}^{N} (x_i^2 k_{x,ij} + y_i^2 k_{y,ij})$, $K_{xy,j} = \sum_{i=1}^{N} x_i y_i k_{x,ij}$, $K_{yx,ji} = \sum_{i=1}^{N} y_i x_i k_{y,ij}$.
If L is the number of storey, the equilibrium equations in terms of the displacement vector are:

$$M\ddot{v} + Kv = 0 \tag{14}$$

$$\upsilon = \begin{bmatrix} \upsilon_1 \\ \vdots \\ \upsilon_L \end{bmatrix}^{\mathrm{T}} \quad M = \begin{bmatrix} M_1 & 0 & \dots & 0 \\ 0 & M_2 & \dots & 0 \\ \vdots & \vdots & \ddots & \vdots \\ 0 & 0 & \dots & M_L \end{bmatrix} \quad K = \begin{bmatrix} K_1 & -K_2 & 0 & \dots & 0 \\ -K_2 & K_1 + K_2 & -K_3 & \dots & 0 \\ \vdots & \vdots & \ddots & \vdots & 0 \\ 0 & 0 & \dots & -K_{L-1} & K_L \end{bmatrix} \tag{15}$$

The modal parameters of this model are obtained from the eigenstructure of Eq.(14).

4.2. Model updating

To measure the distance between the estimated modal parameters and the numerical ones, the following objective function is used [30]:

$$C = \sum_{i=1}^{M} \gamma_i \left(\frac{\omega_i^m - \omega_i^c}{\omega_i^m} \right)^2 + \beta \sum_{i=1}^{M} (1 - diag(MAC(\Phi_i^m, \Phi_i^c))) \tag{16}$$

where the apex $(*)^m$ indicates a measured variable, the apex $(*)^c$ a calculated variable, Φ_i is the mode shape vector, M is the number of modes, MAC is the modal assurance criterion [31], while γ_i and β are weighting factors. The weighting factors are set equal to one. Since the storeys are almost identical among each other, except for the roof, the mass of a generic storey M_{storey}, and that of the roof M_{roof} are set as estimand parameters in the optimization. The main reasons for this choice are:

- The mass is known with greater uncertainty than the geometry and stiffness of the CLT walls, whose properties are known from the producer. Except for the self-weight of the CLT floors, the variable load (people, furniture, e.g.) is almost unknown and non-stationary;
- The optimization of both stiffness and mass, based on the natural frequencies and un-scaled mode shapes, may stand as an undetermined problem: the eigenfrequencies depend on the ratio between rigidity and weight; Theoretically, infinite couples of rigidity and weight values could be possible candidates for the optimization.

The computation of the equivalent rigidity of the CLT walls [32–34] is based on the longitudinal and shear elastic moduli declared by the producer. The bending stiffness is calculated considering only the vertical layers and an equivalent shear modulus takes into account the torsional deformation of the lamellae. Specifically, both the shear and the bending deformation of the walls are taken into account in the following:

$$k_{CLT} = \left(\frac{h^3}{12\,EI} + \frac{1.2h}{GA} \right)^{-1} \tag{17}$$

where h is the inter-storey height, E the Elastic modulus, G the shear modulus and A the cross sectional area of the wall.
To reduce the number of modelling simplifications, the entire mass of the storeys is assumed unknown (M_{storey} e M_{roof}). The authors estimated the minimum of the objective function by evaluating the objective function in a discretized domain with a 0.1 KN step. The contour plot of the objective function is shown in Fig.7, the "X" indicates the minimum of the function. The optimized parameters are itemized in Tab.4.

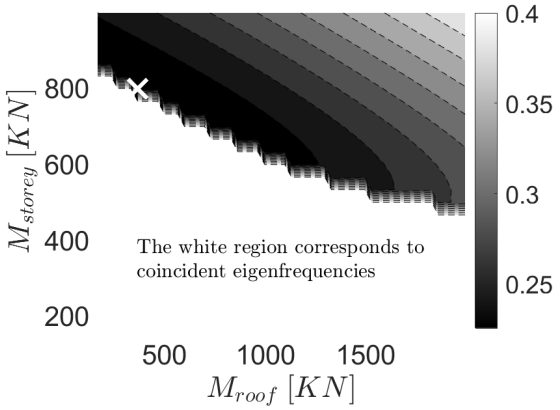

Figure 7: Contour plot of the objective function.

Table 2: Weight values estimated from updating.
Mass

Description	KN	KN/m^2
Roof	365.6	1.042
j-th storey	797.7	2.275
Self Weight of the j-th storey	350.7	1.000
Variable and permanent of the roof	14.9	0.042
Variable and permanent load of the j-th floor	447.0	1.275

Table 3: Comparison between the expected and estimated Self-Weight of the roof

Description	Estimated value	Expected value
Self Weight of the j-th storey [KN/m^2]	1.000	1.100

To evaluate the portion of the storey mass due to the variable and permanent load, the self-weight of the CLT floors is assumed known and subtracted from the M_{storey} and M_{roof} values, Tab.4.
Tab.3 reports the estimated and expected values of the self-weight of the generic floor: the two values are almost coincident. The self-weight of j-th generic floor is

Table 4: Comparison between the experimental and numerical modal parameters.

	Experimental		Numerical	
Mode shapes	**f[Hz]**	ξ **[%]**	**f[Hz]**	**MAC**
1st translational mode	1.913	1.216	1.867	0.99
2nd translational mode	2.414	1.916	2.543	0.98
1st torsional mode	2.693	1.921	2.712	0.92

close to the estimated mass of the roof. This is true, since the sole extra load on the roof was due to the thermal insulation coating and the ventilation system.

5. Discussion

Direct methods or indirect methods can drive the assessment of the role of the connections. The direct method directly estimate the stiffness of the connections by updating all modelling parameters. The indirect method, followed in this paper, derives from proving hypothesis through tests. Let assume a continuum-like behaviour of the building (hypothesis): the connections are neglected in the model updating process (test). If the updated masses match with the expected ones, the hypothesis is proven (proof). In the following part, the authors discuss the causes of the obtained results. Most of the scholars pursue a direct and more conventional approach: a Finite Element Model of the building would have driven the optimization of both the storey masses and the stiffness of the connections. The obtained parameters would have then provided a direct assessment of the role of the connections.

5.1. The role of connections

Comparing the measured natural frequencies with those calculated from the numerical model, it appears that the connections do not significantly contribute to the low-amplitude dynamics. The modal parameters of the numerical model with infinitely rigid connections, in fact, are in great accordance with the experimental ones.

Theoretically, the possible nonlinear response of the building could be evidenced at a very low-level response, when the uplift of the CLT walls arises. Recurring to the experiments by Gavric et al. [9, 35], the ratio between the uplift stiffness at a very first stage, estimated by the tangent to zero of the backbone curve in Fig.8, and the elastic rigidity estimated from Eq.(17) is approximately:

$$r = \frac{k_{uplift}}{k_{elastic}} \approx \frac{11606\,\mathrm{KN/m}}{39387\,\mathrm{KN/m}} = 0.29\% \tag{18}$$

It follows that the CLT building may exhibit important frequency shifts even at the low-level dynamics. This phenomenon (uplift, rocking [36, 37] e.g.) could be easily

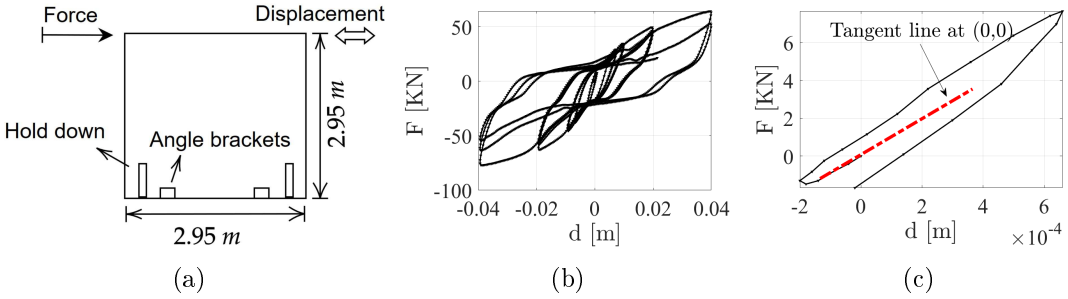

Figure 8: (a) Layout of the CLT panels tested by Gavric et al. [9]; (b) Hysteresis loops of the tested panel; (c) Representation of the first steps of the cyclic tests shown in (b): the dotted line is the tangent to zero.

estimated from continuous monitoring under different operational conditions (e.g. wind speed). Besides, given the difference between the elastic and the uplift rigidity Fig.9, the model updating with a $\approx 0.3\%$ of the elastic stiffness would lead to an non-realistic increment of the storey masses. Fig.9 is an oversimplification, analytical

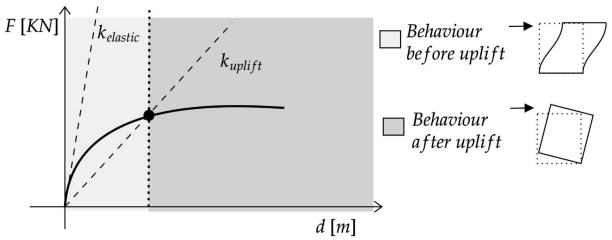

Figure 9: Schematic representation of the CLT wall panel behaviour.

prediction models were discussed by [9, 38]. According to Gavric et al. [9] the lateral displacement on top of a CLT wall can be divided into several contributions: (i) rocking deformation, (ii) sliding deformation, (iii) bending deformation, (iv) shear deformation. However, the incremental deformation due to vertical elongation of the wall anchorage, which is further considered by the Canadian Standard Association [39], is likely to be negligible in operational conditions.

5.2. Correlations to the building height

As evidenced in the previous section, several factors, peculiar of the considered CLT building, may determine the eigenfrequencies in Tab.4:

- Negligible influence of the connections in the very low intensity dynamics;
- High stiffness to weight ratio of CLT panels;

- Redundancy of structural components [13].

The straightforward estimation of the first natural frequency may be important for practitioners: to perform static seismic analyses, in fact, national codes provide a simplified equation for estimating the main frequency of a structure.
The formulations proposed by ASCE 07-16 (2017) [40] and the former Italian Seismic Code [41] are similar (Eq.(19)), while that of the Spanish Code [42] is more complete Eq.(20):

$$f_1(H) = \frac{1}{C_1 H^{3/4}} \tag{19}$$

$$f_1(H) = \frac{\sqrt{H}}{C_2 H \sqrt{\frac{H}{(2L+H)}}} \tag{20}$$

where C_1 and C_2 are constants, H is the building height in metres, L the plan dimension along the direction of oscillation in metres. The current Italian Seismic Code [43] proposes a different formulation:

$$f_1(d) = \frac{1}{2\sqrt{d}} \tag{21}$$

where d is the lateral elastic displacement of the highest point of the structure under the seismic action. The constants C_1, computed by setting f_1 equal to the first experimental eigenfrequency, and C_2, estimated from an Ordinary Least Squares Operator are reported in Tab.5. C_1 is very close to the proposed value for masonry

Table 5: Estimated constants of Eq.(19)-(20) based on the results in Tab.4.

C_1	0.0443
C_2	0.1100

$C_1 = 0.0488$. This might be due to the sharing of a wall-based structure in both typologies, CLT and masonry. It must be remarked that the use of the first eigenfrequency based on simplified formulations is mainly devoted to static linear analysis; Static linear analysis are highly conventional approaches, given the uncertainties on the seismic action estimation and the linear approximations of the structural behaviour.

5.3. Damping estimation

The damping factors estimated by Reynolds at al. [5], which span in the range 4.7-7%, are sensibly higher than those in Tab.4. In particular, the damping factors of the building under test are very close to the damping of timber itself, which is about 2%. However, the building tested by [5] has a RC core, while the current

building has a CLT one. Hence, the RC core might sensibly increase the damping factor, from that of CLT to that of concrete.

6. Conclusions

The results of the dynamic identification in operational conditions of an eight-storey CLT building are interpreted in the light of an elementary analytical model. Three stable modes are detected, two translational and one torsional: the diaphragm-like behaviour of the CLT floors is clearly evidenced by the mode shapes. The analytical model is calibrated on the experimental eigenstructure using a proper objective function, whose estimand parameters were the masses of the storeys. Given the accordance with the analytical model, the building is likely to behave linearly at a very low vibration level, when the contribution of the connections is not activated. However, the contribution of the connections to the global dynamics may possibly be observed by continuous dynamic monitoring under different vibration-induced levels. The first eigenfrequency matches well with that estimated from empirical relations tuned to masonry structures: this may be due to the wall-based construction typology, recurring in both masonry and CLT structures. The damping factors, which span in the range 1.2-1.9%, are very close to those of timber.
The authors will attempt to further investigate the behaviour of tall CLT buildings from Continuous Dynamic Monitoring of this structure.

7. Acknowledgements

The authors thank Andreas S. Fløe, SiÅs and Thomas K. Thiis for their kind support.

References

[1] A. Aloisio, M. Fragiacomo, and G. D'Alò, "The 18th-century baraccato of l'aquila," *International Journal of Architectural Heritage*, pp. 1–15, 2019.

[2] A. Aloisio, M. Fragiacomo, and G. D'Alò, "Traditional tf masonries in the city centre of l'aquila–the baraccato aquilano," *International Journal of Architectural Heritage*, pp. 1–18, 2019.

[3] R. Brandner, G. Flatscher, A. Ringhofer, G. Schickhofer, and A. Thiel, "Cross laminated timber (clt): overview and development," *European Journal of Wood and Wood Products*, vol. 74, no. 3, pp. 331–351, 2016.

[4] M. Izzi, D. Casagrande, S. Bezzi, D. Pasca, M. Follesa, and R. Tomasi, "Seismic behaviour of cross-laminated timber structures: A state-of-the-art review," *Engineering Structures*, vol. 170, pp. 42–52, 2018.

[5] T. Reynolds, D. Casagrande, and R. Tomasi, "Comparison of multi-storey cross-laminated timber and timber frame buildings by in situ modal analysis," *Construction and Building Materials*, vol. 102, pp. 1009–1017, 2016.

[6] T. Reynolds, R. Harris, W.-S. Chang, J. Bregulla, and J. Bawcombe, "Ambient vibration tests of a cross-laminated timber building," *Proceedings of the Institution of Civil Engineers-Construction Materials*, vol. 168, no. 3, pp. 121–131, 2015.

[7] T. Reynolds, R. Harris, and W. Chan, "Dynamic response of tall timber buildings to wind load," in *35th Annual Symposium of IABSE/52nd Annual Symposium of IASS/6th International Conference on Space Structures, London*, 2011.

[8] I. Mugabo, A. R. Barbosa, and M. Riggio, "Dynamic characterization and vibration analysis of a four-story mass timber building," *Frontiers in Built Environment*, vol. 5, p. 86, 2019.

[9] I. Gavric, M. Fragiacomo, and A. Ceccotti, "Cyclic behavior of clt wall systems: Experimental tests and analytical prediction models," *Journal of Structural Engineering*, vol. 141, no. 11, p. 04015034, 2015.

[10] A. Ceccotti, C. Sandhaas, M. Okabe, M. Yasumura, C. Minowa, and N. Kawai, "Sofie project–3d shaking table test on a seven-storey full-scale cross-laminated timber building," *Earthquake Engineering & Structural Dynamics*, vol. 42, no. 13, pp. 2003–2021, 2013.

[11] G. Rinaldin and M. Fragiacomo, "Non-linear simulation of shaking-table tests on 3-and 7-storey x-lam timber buildings," *Engineering Structures*, vol. 113, pp. 133–148, 2016.

[12] M. Follesa, I. Christovasilis, D. Vassallo, M. Fragiacomo, and A. Ceccotti, "Seismic design of multi-storey clt buildings according to eurocode 8. ingegneria sismica," *International Journal of Earthquake Engineering, Special Issue on Timber Structures*, vol. 30, 2013.

[13] I. Lukacs, A. Björnfot, T. Tsalkatidis, and R. Tomasi, "Structural redundancy in cross-laminated timber buildings," *Proceedings of the World Conference on Timber Engineering WCTE2016*.

[14] A. Aloisio, R. Alaggio, and M. Fragiacomo, "Dynamic identification of a masonry façade from seismic response data based on an elementary ordinary least squares approach," *Engineering Structures*, vol. 197, p. 109415, 2019.

[15] A. Aloisio, L. Di Battista, R. Alaggio, and M. Fragiacomo, "Analysis of the forced dynamics of a masonry facade by means of input-output techniques and a linear regression model," in *COMPDYN, 2019, 7th International Conference on Computational Methods in Structural Dynamics and Earthquake Engineering*, 2019.

[16] R. Alaggio, D. Galeota, E. Antonacci, and A. Aloisio, "The s. maria di collemaggio basilica: from the vulnerability assessment tothe first results of shm.," *Atti del XVIII Convegno ANIDIS L'ingegneria Sismica in Italia*, pp. 75–85, 2019.

[17] M. Aoki, *State space modeling of time series*. Springer Science & Business Media, 2013.

[18] K. Arun and S. Kung, "Balanced approximation of stochastic systems," *SIAM journal on matrix analysis and applications*, vol. 11, no. 1, pp. 42–68, 1990.

[19] B. Peeters and G. De Roeck, "Reference-based stochastic subspace identification for output-only modal analysis," *Mechanical systems and signal processing*, vol. 13, no. 6, pp. 855–878, 1999.

[20] A. Aloisio, L. Di Battista, R. Alaggio, and M. Fragiacomo, "Sensitivity analysis of subspace-based damage indicators under changes in ambient excitation covariance, severity and location of damage," *Engineering Structures*, vol. 208, p. 110235, 2020.

[21] A. Aloisio, L. Di Battista, R. Alaggio, E. Antonacci, and M. Fragiacomo, "Assessment of

structural interventions using bayesian updating and subspace-based fault detection methods: the case study of s. maria di collemaggio basilica, l'aquila, italy," *Journal Structure and Infrastructure Engineering*, 2020.

[22] A. A. Antonacci, E., D. Galeota, and R. Alaggio, "The s. maria di collemaggio basilica: from vulnerability assessment to first results of shm," *Journal of Archiectural Engineering*, vol. Forthcoming, p. in press, 2020.

[23] M. Döhler and L. Mevel, "Subspace-based fault detection robust to changes in the noise covariances," *Automatica*, vol. 49, no. 9, pp. 2734–2743, 2013.

[24] M. Döhler, P. Andersen, and L. Mevel, "Data merging for multi-setup operational modal analysis with data-driven ssi," in *Structural Dynamics, Volume 3*, pp. 443–452, Springer, 2011.

[25] E. Reynders, R. Pintelon, and G. De Roeck, "Uncertainty bounds on modal parameters obtained from stochastic subspace identification," *Mechanical systems and signal processing*, vol. 22, no. 4, pp. 948–969, 2008.

[26] B. EN, "1-1: 2004 eurocode 5: Design of timber structures—general—common rules and rules for buildings," 1995.

[27] A. K. Chopra, *Dynamics of structures theory and*. 1995.

[28] G. Tamagnone, G. Rinaldin, and M. Fragiacomo, "Influence of the floor diaphragm on the rocking behavior of clt walls," *Journal of Structural Engineering*, vol. 146, no. 3, p. 04020010, 2020.

[29] G. Tamagnone, G. Rinaldin, and M. Fragiacomo, "A novel method for non-linear design of clt wall systems," *Engineering Structures*, vol. 167, pp. 760–771, 2018.

[30] M. Friswell and J. E. Mottershead, *Finite element model updating in structural dynamics*, vol. 38. Springer Science & Business Media, 2013.

[31] R. J. Allemang and D. L. Brown, "A correlation coefficient for modal vector analysis," in *Proceedings of the 1st international modal analysis conference*, vol. 1, pp. 110–116, SEM Orlando, 1982.

[32] H. J. Blass and P. Fellmoser, "Design of solid wood panels with cross layers," in *8th world conference on timber engineering*, vol. 14, p. 2004, 2004.

[33] F. Boggian, M. Andreolli, and R. Tomasi, "Cross laminated timber (clt) beams loaded in plane: testing stiffness and shear strength," *Frontiers in Built Environment*, vol. 5, p. 58, 2019.

[34] I. Lukacs, A. Björnfot, and R. Tomasi, "Strength and stiffness of cross-laminated timber (clt) shear walls: State-of-the-art of analytical approaches," *Engineering Structures*, vol. 178, pp. 136–147, 2019.

[35] A. Aloisio, R. Alaggio, K. Jochen, and M. Fragiacomo, "Extension of the generalized bouc-wen hysteresis modelling of wood joints and structural systems," *Journal of engineering mechanics*, vol. 146, no. 3, 2020.

[36] A. Di Egidio, R. Alaggio, A. Aloisio, A. M. de Leo, A. Contento, and M. Tursini, "Analytical and experimental investigation into the effectiveness of a pendulum dynamic absorber to protect rigid blocks from overturning," *International Journal of Non-Linear Mechanics*, vol. 115, pp. 1–10, 2019.

[37] P. Stefano, A. Angelo, D. E. Angelo, and A. Rocco, "Investigation into benefits of coupling a frame structure with a rocking rigid block," in *XXIV Congresso AIMETA 2019, Associazione Italiana di Meccanica Teorica e Applicata*, 2019.

[38] D. Casagrande, S. Rossi, T. Sartori, and R. Tomasi, "Proposal of an analytical procedure and a simplified numerical model for elastic response of single-storey timber shear-walls," *Construction and Building Materials*, vol. 102, pp. 1101–1112, 2016.

[39] T. Tannert and P. Eng, "Design provisions for cross-laminated timber structures," in *Structures Congress 2019: Buildings and Natural Disasters*, pp. 171–178, American Society of Civil Engineers Reston, VA, 2019.

[40] A. S. of Civil Engineers, "Minimum design loads and associated criteria for buildings and other structures," American society of civil engineers, 2017.

[41] M. d. I. e dei Trasporti, "Ntc2008–norme tecniche per le costruzioni," tech. rep., DM 14/01/2008 [In Italian], 2008.

[42] D. C. S. NORMA, "Parte general y edificación (ncse-02)," *BOE*, vol. 244, no. 11.10, p. 02, 2002.

[43] N. T. per le Costruzione, "Aggiornamento delle norme tecniche per le costruzioni," tech. rep., decreto 17-1-2018, Gazzetta Ufficiale 42, 20-02-2018, Ordinary Suppl, 2018.

List of Figures